Journal of the Physical Society of Japan
Vol. 75, No. 5, May, 2006, 054603

Quantum Statistical Approach to Debye-Waller Factor in EXAFS, EELS, and ARXPS: VII. Path Integral Approach to Asymmetric Double-well Potentials

Kiyofumi NITTA*, Takafumi MIYANAGA and Takashi FUJIKAWA[1]

Department of Advanced Physics, Faculty of Science and Technology, Hirosaki University, 3 Bunkyo-cho, Hirosaki, Aomori 036-8561
[1]*Graduate School of Science, Chiba University, 1-33 Yayoi-cho, Inage, Chiba 263-8522*

(Received November 8, 2005; accepted March 10, 2006; published May 10, 2006)

We apply a finite temperature path integral method to study strongly anharmonic thermal factors in extended X-ray absorption fine structure (EXAFS), electron energy-loss spectroscopy (EELS) and angle resolved X-ray photoelectron spectroscopy (ARXPS). Two examples, symmetric and asymmetric double-well potentials are considered for the anharmonic potentials, which are used to describe structural phase transition and rattling mechanism. We discuss the quantum tunneling effects in the thermal factors. The validity of the classical approximation and the cumulant expansion are also studied for various asymmetric potentials. Complex plane expression is introduced to explain the specific features of the EXAFS thermal damping function. Degree of asymmetry of the potential can be estimated from the complex plane expression. In the temperature dependence of the higher order cumulant (third and fourth), minimum point (third order) and maximum point (fourth order) appear at the characteristic temperature, which depends on the potential asymmetry.

KEYWORDS: EXAFS, Debye-Waller factors, double-well potential, path-integral, cumulant expansion, damping function
DOI: 10.1143/JPSJ.75.054603

1. Introduction

Thermal factors in core spectroscopies such as EXAFS, EELS, and ARXPS are important to study local atomic structures around an excited atom. They also provide useful information about atomic vibration.

Theoretical aspects of temperature dependence in EXAFS were first studied by Beni and Platzman[1] within the framework of harmonic vibration for nuclei motion and plane wave approximation for photoelectron waves. Since that time some improvements have been found beyond the harmonic approximation[2–5] and the plane wave approximation.[6,7] When they include the anharmonic effects in EXAFS analyses, perturbation theory has been applied by use of temperature Green's function[3] or thermal perturbation theory. The former approach has been applied to infinite crystals,[4] and the latter to finite clusters.[8] These perturbation approaches are useful to describe weak anharmonicity in the analyses of temperature effects in EXAFS, EELS, ARXPS spectra, and they have provided interesting information based on cumulant expansion.

On the other hand real space approach proposed by Yokoyama *et al.*[9] has been used to relate the EXAFS thermal factors to interatomic potential. In those analyses the original interatomic potential is used, that is, the classical approximation is used. It can be safely used in high temperature region even though the anharmonicity is strong. Whether we can apply this approach to the analyses at low temperature region with minor modification or not is still one of open questions.

The perturbation method mentioned above are useful for weak anharmonicity, however they cannot be applied to strong anharmonic systems. For the EXAFS analyses of thermal effects in double-well potential, a different approach should be inevitably used instead of the perturbation method. To study this kind of problem, Mustre de Leon and his collaborators have used a double-well potential,[10]

$$V(z) = a(z - z_1)^2 \ (z \geq z_0), \quad b(z - z_2)^2 \ (z \leq z_0) \qquad (1)$$

where a, b, z_1, and z_2, are fitting parameters. This potential easily gives the probability density $P(z)$ which has two peaks even at low temperature. The main drawback of this potential is that the potential can be continuous at $z = z_0$, but its derivative is not continuous at that point.

Our previous papers (I–IV)[3–6] have studied weak anharmonic systems based on a perturbation approach and cumulant expansion. The papers V[11] and VI[12] discuss a real space approach to study EXAFS thermal factor based on the finite temperature path-integral method originally developed by Feynman,[13] later improved by Cuccoli *et al.*,[14] and also Feynman and Kleinert.[15] This self-consistent approach can be applied to strongly anharmonic systems and can be closely related to the classical formulas. We have studied the range of the applicability of widely used cumulant analyses and of the classical approximation for the EXAFS thermal factors.[11,16] The effective potential method by Yokoyama[17] and path-integral Monte Carlo (PIMC) method by Fornasini and coworkers[18] have also been successfully applied to EXAFS thermal analyses.

In this paper we apply the path-integral effective potential method to one-dimensional symmetric and asymmetric double-well potential systems in a reservoir at temperature T. For these systems conventional cumulant analyses do not work well. To obtain good convergence for these systems, we should improve the numerical calculation at low temperature. In $PbTiO_3$, atomic pair potential function is well approximated by asymmetric double-well potential which can describe "soft mode" behavior.[19] Doll *et al.* studied

*E-mail: h03gs213@cc.hirosaki-u.ac.jp

some thermodynamical properties of small clusters by use of Fourier Path Integral analyses,[20] in which atomic pair potential function is also considered as asymmetric double-well potential. In the filled skutterudites, $PrOs_4Sb_{12}$ is known as 4f heavy fermion superconductor and shows an interesting rattling behavior suggested by ultrasonic measurement[21] in which Pr ion is considered to be moving in the double-well potential in the cage of Sb_{12}.

In these examples, the double-well potential is only phenomenologically introduced to explain the observed results. The Debye-Waller factors in EXAFS are sensitive to the shape of the pair potential between the X-ray absorbing atom and the surrounding atoms. For example, the EXAFS envelop function for the symmetric double-well potential shows its specific feature.[11] It is thus interesting to study the EXAFS Debye-Waller factors for asymmetric double-well potentials. To analyze the Debye-Waller factor in EXAFS is important, because it makes possible to directly observe the existence of the double-well potential and further to evaluate the shape of that potential. The present approach should be useful for the structural studies of new materials to show exotic physical properties in which atoms are driven by double-well potential.

2. Theory

Let consider diatomic systems in a reservoir whose relative vibrational motion is described by the Hamiltonian,

$$H = \frac{p^2}{2\mu} + V(q) \tag{2}$$

where μ is the reduced mass and q is the instantaneous interatomic distance. When we deal with statistical average of an operator A, we should calculate the trace,

$$\langle A \rangle = \frac{1}{Z}\mathrm{Tr}(A\rho) \tag{3}$$

where ρ is the density operator defined by $\rho = \exp(-\beta H)$, $(\beta = 1/k_B T)$ and $Z = \exp(-\beta F) = \mathrm{Tr}(\rho)$ is the partition function for the systems. The trace can be calculated by applying Feynman's path-integral techniques, however, instead of summing over all paths in just one step, one can classify the paths into two groups as proposed by Feynman.[13] One group consists of average (quasi classical) path $\bar{q}$ given by

$$\bar{q} = \frac{1}{\beta}\int_0^\beta q(u)\,\mathrm{d}u, (\hbar = 1) \tag{4}$$

and the other group consists of quantum fluctuation around $\bar{q}$. The average path is the same as the classical path in the high temperature limit ($\beta \to 0$). To use the non-perturbation method based on the path-integral techniques, we approximate the instantaneous potential $V(q(u))$ by a trial potential quadratic in the fluctuation path $q - \bar{q}$,[13,14]

$$V \cong V_0(q, \bar{q}) = w(\bar{q}) + \frac{\mu\omega(\bar{q})^2}{2}(q - \bar{q})^2. \tag{5}$$

Now the parameter $w(\bar{q})$ and $\omega(\bar{q})$ are to be optimized so that the trial reduced density $P(q)$ well approximates the true reduced density. A variational approach which gives the same result as the self-consistent approximation is also possible.[13,14] Final expression for the average of a local operator A can be represented in terms of the probability density $P(q)$ just like a classical statistical mechanics (from now on q is used instead of $\bar{q}$ for brevity),

$$\langle A \rangle = \int A(q)P(q)\,\mathrm{d}q. \tag{6}$$

This expression, however, includes important quantum effects, and the probability is represented by

$$P(q) = \frac{1}{Z}\sqrt{\frac{\mu}{2\pi\beta}}\exp[-\beta V_{\mathrm{L}}(q)], \tag{7}$$

where local effective potential $V_{\mathrm{L}}(q)$ is defined by

$$\exp[-V_{\mathrm{L}}(q)] = \int \mathrm{d}\xi \exp[-V_{\mathrm{e}}(q+\xi)] \times \frac{1}{\sqrt{2\pi\alpha(q+\xi)}}\exp\left[-\frac{\xi^2}{2\alpha(q+\xi)}\right]. \tag{8}$$

Now we have used the relations,

$$V_{\mathrm{e}}(q)/\varepsilon = w(q) + \frac{1}{\beta}\ln\left(\frac{\sinh f(q)}{f(q)}\right), \tag{9}$$

$$f(q) = \frac{\beta\omega(q)}{2}, \tag{10}$$

$$\alpha(q) = (\coth f(q) - 1/f(q))/(2\mu\omega(q)), \tag{11}$$

where ε is the energy scale. The local effective potential $V_{\mathrm{L}}(q)$ is reduced to the bare potential $V(q)$ in the high temperature limit.

In the EXAFS analyses the operator A should be $\exp(2ik\Delta_\alpha)$ where k is the wave vector of ejected photoelectrons, $k = |\mathbf{k}|$ and Δ_α is the projected relative displacement, which is simply given by $\Delta_\alpha = \Delta q = q - q_0$ in one-dimensional cases; q_0 is the equilibrium interatomic distance. So that what we should calculate to study EXAFS thermal factor is the thermal average including quantum fluctuation given by

$$\langle \exp(2ik\Delta q)\rangle = \frac{1}{Z}\sqrt{\frac{\mu}{2\pi\beta}}\int \exp(2ik\Delta q)\exp[-\beta V_{\mathrm{L}}]\,\mathrm{d}q. \tag{12}$$

Any order of moments $\langle q^n \rangle$ is also calculated by use of the local effective potential $V_{\mathrm{L}}(q)$

$$\langle q^n \rangle = \frac{1}{Z}\sqrt{\frac{\mu}{2\pi\beta}}\int q^n \exp[-\beta V_{\mathrm{L}}(q)]\,\mathrm{d}q. \tag{13}$$

We now shifted the origin for the potential $V(q)$ to be $q_0 = 0$. This expression shows that the widely used real space representation is obtained with some modification from the quantum fluctuation effects: the original interatomic potential $V(q)$ should be replaced by the local effective potential $V_{\mathrm{L}}(q)$ which is temperature dependent and tends to be $V(q)$ at high temperature from physical consideration. Though the discussion is only shown for the EXAFS thermal factors here, extension to EELS and ARXPS thermal factors is straightforward.[11]

3. Results and Discussion

In this section the method described in the previous section is applied to anharmonic diatomic systems in double-well potentials given by

$$V(q)/\varepsilon = v(q) = (q^2 - \sigma^2)^2 + c\sigma\left(\frac{q^3}{3} - \sigma^2 q\right), \tag{14}$$

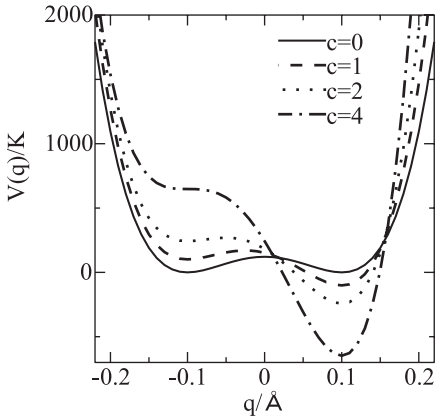

Fig. 1. The double-well potential $V(q) = (q^2 - \sigma^2)^2 + c\sigma(\frac{q^3}{3} - \sigma^2 q)$, $(c = 0, 1, 2, 4)$ for fixed σ: $\sigma = 0.1$ Å.

where σ is the minima of the potential well and c is the measure of asymmetry of the double-well potential: The strongly asymmetric potential is obtained for the large c. This potential has the absolute minimum at $q = \pm\sigma$ irrespective of c. We introduced a parameter g defined by

$$g = \sqrt{\frac{\hbar^2 v''(q_{\min})}{\mu\varepsilon\sigma^2}}. \tag{15}$$

Small (large) g value gives rise to a weak (strong) quantum effect. By use of this parameter g, we define a reduced temperature t by

$$t = \frac{k_B T}{\varepsilon} = \left(\frac{\hbar^2 v''(q_{\min})}{\mu g^2 \sigma^2}\right)^{-1} k_B T. \tag{16}$$

In the present paper we use energy scale ε and length scale σ for Cu–O in high-temperature superconductor $YBa_2Cu_3O_{7-\delta}$,[22] which is a model for double-well potential. Figure 1 shows the double-well potential for various c values at $\sigma =$ 0.1 Å.

Mustre de Leon *et al.*[10] considered a similar asymmetric quartic potential

$$V(q) = \left[\frac{a}{2}q^2 + \frac{b}{4}q^4 + \frac{c}{\sqrt{2}}q^3\right]e^{-d|q/2|} \tag{17}$$

which represents a single-well potential ($a > 0$, $b > 0$) or a double-well potential ($a < 0$, $b < 0$). They introduced the exponential factor to avoid the unphysical behavior $V(q) \to q^4$ for large q. On the other hands, in the present double-well potential, the values of potential minima, σ, do not depend on the asymmetry of the potential. Although they disucussed the quantum statistical wave function, they only obtained parameters of the asymmetric potential by fitting to the experimental EXAFS radial distribution function, which was obtained from the bare potential $V(q)$ on the basis of classical statistics. They evaluated the quantum effect as tunneling frequency $\hbar\omega_t = \varepsilon_1 - \varepsilon_0$, where ε_1 and ε_0 were first excited and ground state energies, respectively. Our methodology is quite different from theirs: the quantum effect is directly evaluated from the quantum effective potential based on the first principle path-integral approach. The probability density $P(q)$ implicitly includes the quantum tunneling effect.

By use of the self-consistent method described in §2, we obtain $f(q)$ as a function of q from which we calculate $V_e(q)$ and $P(q)$.

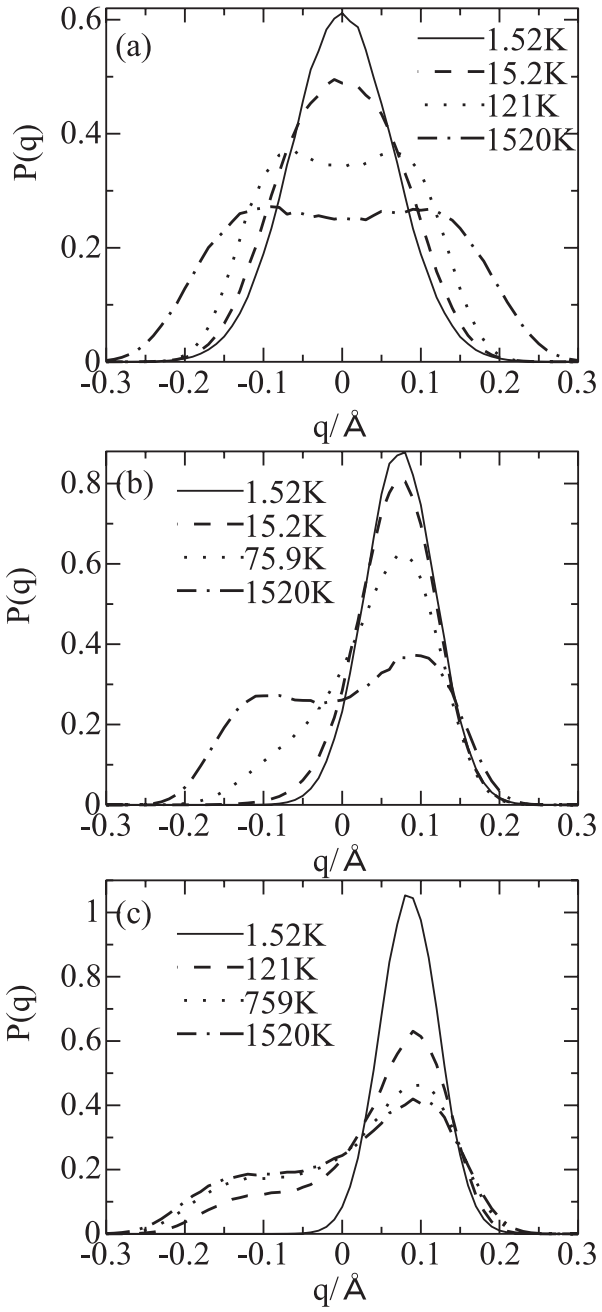

Fig. 2. The probability density $P(q)$ for different asymmetry parameter c and temperatures T; (a) $c = 0$, (b) $c = 1$, (c) $c = 4$.

Figure 2 shows the quantum probability density $P(q)$ for different $c = 0$ (a), 1 (b), 4 (c). In the case of symmetric double-well potential ($c = 0$), $P(q)$ has a single peak around $q = 0$ Å at low temperature ($T = 1.52$ and 15.2 K) because of the tunneling effect, but it is split into two peaks at $q = \pm 0.1$ Å for the higher temperature. In classical picture nuclear position is frozen at $q = \pm 0.1$ Å, at the bottoms of the deep potential holes. The asymmetric double-well potentials ($c = 1$ and 4) give also single peak at low temperature ($T = 1.52$ and 15.2 K), but the peak position is not at $q = 0.1$ Å and shifted to smaller q even in low temperature because the tunneling probability from the deeper bottom to the shallow bottom is already finite. As temperature increases, the two peaks are found at $q = 0.1$ Å

and at $q = -0.1$ Å because of thermal excitation to the shallow bottom at $q = -0.1$ Å.

3.1 Temperature dependence of cumulants in EXAFS thermal factor

From eqs. (7) and (13) we can evaluate the second, third, and fourth order cumulants $\langle \ldots \rangle_c$ by use of the same and lower order moments,

$$\langle q \rangle_c = \langle q \rangle, \tag{18}$$

$$\langle q^2 \rangle_c = \langle q^2 \rangle - \langle q \rangle^2, \tag{19}$$

$$\langle q^3 \rangle_c = \langle q^3 \rangle - 3\langle q \rangle \langle q^2 \rangle + 2\langle q \rangle^3, \tag{20}$$

$$\langle q^4 \rangle_c = \langle q^4 \rangle - 4\langle q^3 \rangle \langle q \rangle - 3\langle q^2 \rangle^2 + 12\langle q^2 \rangle \langle q \rangle^2 - 6\langle q \rangle^4. \tag{21}$$

Figure 3(a) shows the first order moment $\langle q \rangle$ as a function of temperature calculated by use of the quantum (solid lines) and the classical (dashed lines) probability density for $c = 1$. The first order moments $\langle q \rangle$ are nearly the same for classical and quantum calculations in high temperature region ($T > 1000$ K), but quantum results are smaller than the classical ones at $T < 1000$ K. Figure 3(b) shows quantum (solid line) and classical (dashed line) probability density at $T = 1.52$ K. In the classical approximation particles are frozen at the deeper bottom of the potential-well ($q = 0.1$ Å), so the probability density has sharp peak at $q = 0.1$ Å, which gives $\langle q \rangle \approx 0.1$ Å at $T = 1.52$ K. In quantum case, the tunneling effect and zero-point vibration play an important role, so that $P(q)$ has a broad peak which shifts to potential barrier side; $\langle q \rangle \approx 0.075$ Å at $T = 1.52$ K.

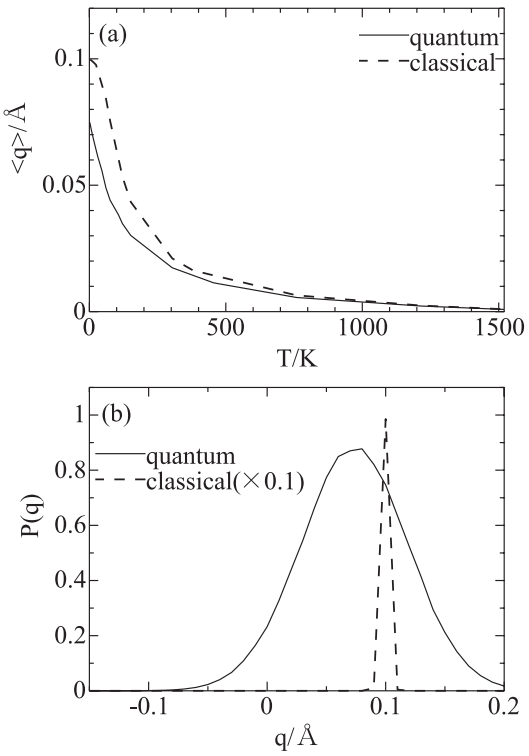

Fig. 3. The temperature dependence of the quantum (solid line) and classical (dashed line) first order moment $\langle q \rangle$ for $c = 1$ (a). The quantum and classical probability density $P(q)$ at $T = 1.52$ K is shown in (b).

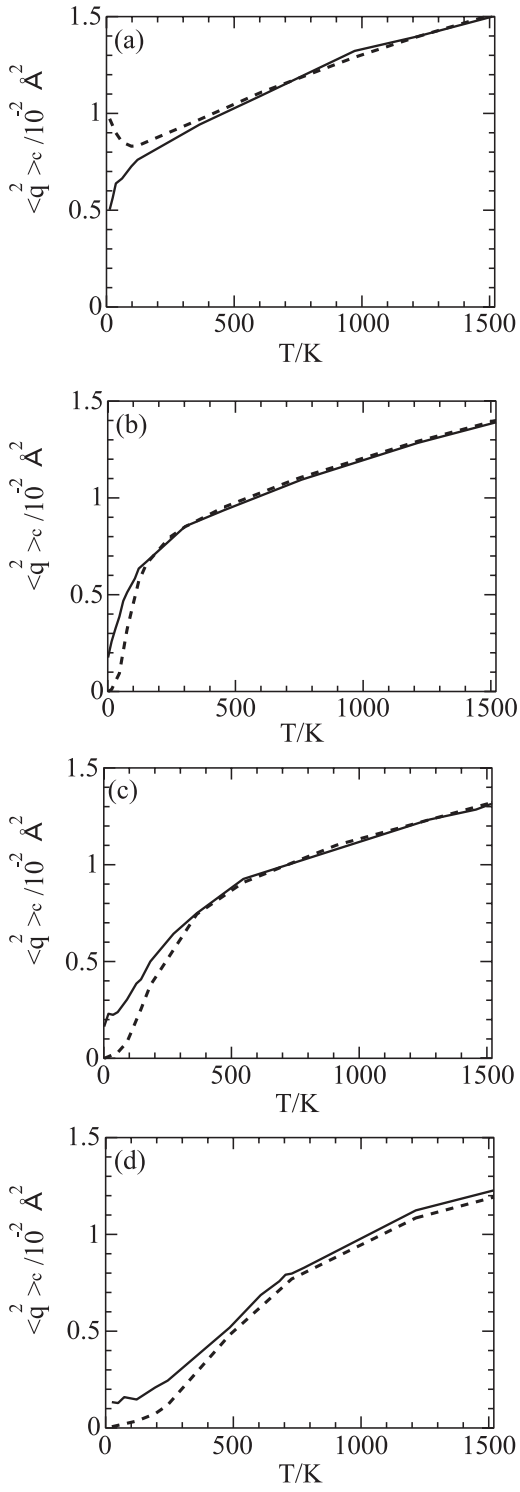

Fig. 4. The temperature dependence of the quantum (solid lines) and classical (dashed lines) second order cumulant $\langle q^2 \rangle_c$ for four different double-well potentials; (a) $c = 0$, (b) $c = 1$, (c) $c = 2$ and (d) $c = 4$.

Figure 4 shows the second order cumulant $\langle q^2 \rangle_c$ as a function of temperature for various double-well potentials, $c = 0$ (a), $c = 1$ (b), $c = 2$ (c) and $c = 4$ (d). The classical approximation gives good result at high temperature [$T > 600$ K for $c = 0$ (a), $T > 200$ K for $c = 1$ (b), $T > 300$ K for $c = 2$ (c), $T > 500$ K for $c = 4$ (d)]. As temperature decreases, the classical probability density has a sharp peak as shown in Fig. 3(b) and the classical approximation gets poor. In particular, for a symmetric potential ($c = 0$) the

classical approximation gives two sharp peaks at ± 0.1 Å in the probability density at $T \sim 0$ K.[11] Thus the classical second order cumulant $\langle q^2 \rangle_c$ approaches to 0.01 Å^2 and gives the largest difference from the quantum result.

At low temperature atoms vibrate near the bottom of the deep potential well and the vibration can be approximated by harmonic vibration, where $\langle q^2 \rangle_c \approx \hbar/\mu\omega$ from Virial theorem. The frequency ω^2 is related to $v''(\sigma) = 8\sigma^2 + 2\sigma^2 c$ for the potential given by eq. (14). As the parameter c increases, $v''(\sigma)$ and ω also increase. As a result $\langle q^2 \rangle_c$ decrease at low temperature as observed in Fig. 4.

Figure 5 shows the third order cumulant $\langle q^3 \rangle_c$ as a function of temperature for three different double-well potentials $c = 1$ (a), $c = 2$ (b), and $c = 4$ (c). In the case of the symmetric double-well potential ($c = 0$), both quantum and classical third order cumulant $\langle q^3 \rangle_c = 0$ irrespective of temperature, because both the classical potential and quantum local effective potential $V_L(q)$ are symmetric. The third order cumulant $\langle q^3 \rangle_c$ reflects asymmetry of the potential. In the case of $c = 1$ and $c = 2$, $\langle q^3 \rangle_c$ shows minimum ($|\langle q^3 \rangle_c|$ is the largest) indicated by arrows at $\sim$100 and $\sim$550 K in quantum calculations. The largest asymmetric distribution is found there (see also Fig. 2). In higher temperature region, the quantum local effective potential is reduced to the bare potential $V(q)$, so $\langle q^3 \rangle_c$ shows the same behavior at high temperature for the quantum and classical calculations. We should note that quantum and classical third order cumulants $\langle q^3 \rangle_c$ are nearly the same for $c = 4$, because the quantum tunneling probability is expected to be quite small as shown in Fig. 2. This characteristic temperature at the minimum position of the third order cumulant shifts to higher when c increases. If we study the temperature dependence of third order cumulant for certain double-well potential, we can obtain some information on the asymmetry of the effective potential $V_L(q)$.

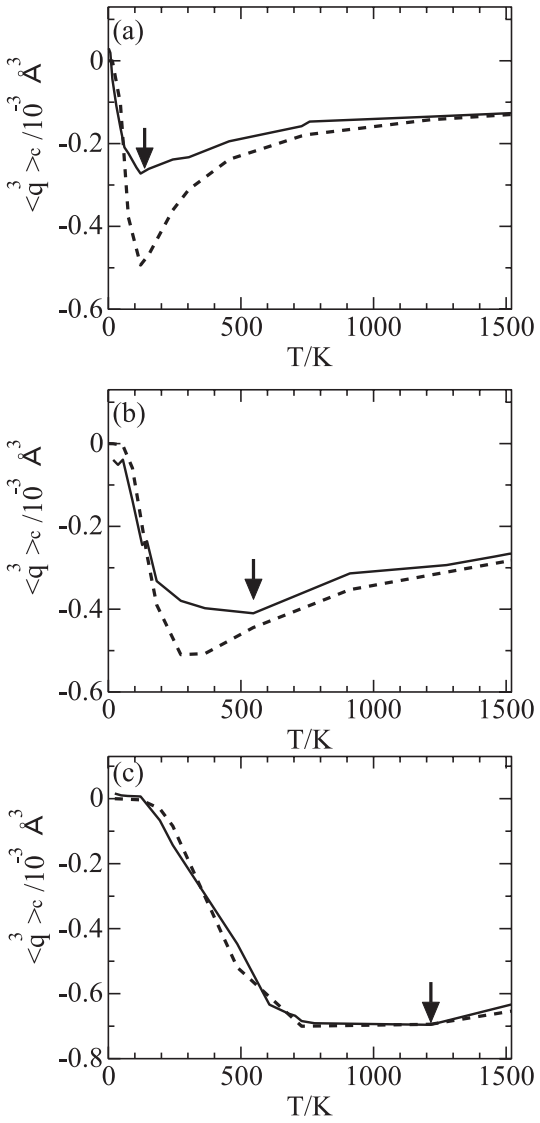

Fig. 5. The temperature dependence of the quantum (solid lines) and classical (dashed lines) third order cumulants $\langle q^3 \rangle_c$ for three different double-well potentials; (a) $c = 1$, (b) $c = 2$ and (c) $c = 4$. The arrows indicate the minimum points, T_m.

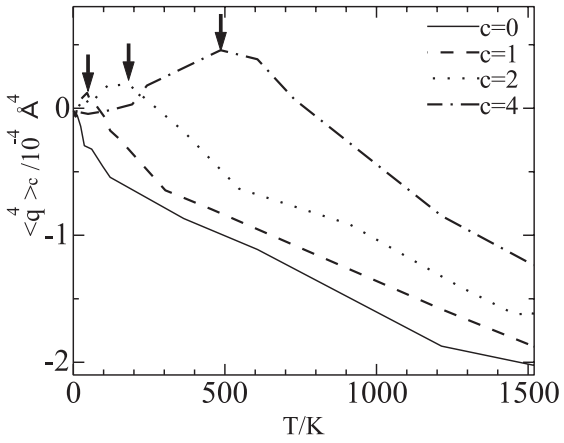

Fig. 6. The temperature dependence of the quantum fourth order cumulant $\langle q^4 \rangle_c$ for four double-well potentials; $c = 0$ (solid line), $c = 1$ (dashed line), $c = 2$ (dotted line), and $c = 4$ (dash-dotted line). The arrows indicate the maximum points, T_m.

Similar behavior is observed in the fourth order cumulant $\langle q^4 \rangle_c$ (in this case, maximum point). Figure 6 shows quantum fourth order cumulant $\langle q^4 \rangle_c$ for four different double-well potentials $c = 0$ (solid line), $c = 1$ (dashed line), $c = 2$ (dotted line), and $c = 4$ (dash-dotted line) as a function of temperature. We also find that the maximum peak position shifts to higher temperature as c. These characteristic features can be used to study the asymmetry of the potential.

Next we discuss the quantum effect in the cumulants for various g values defined by eq. (15). Figure 7 shows the second, third, and fourth order quantum cumulants for various g values as functions of reduced temperature t defined by eq. (16), and classical cumulants for comparison. In the case of $g = 1$ (weak quantum case), the quantum calculations provide similar curves to the classical cumulants even in quite low temperature. In the case of $g = 5$ and $g = 10$, quantum calculations shows large difference from classical curves as expected, in particular for the third order cumulants.

3.2 *EXAFS thermal damping function*

In this section, we discuss EXAFS thermal damping function $G(k)$ defined by[11]

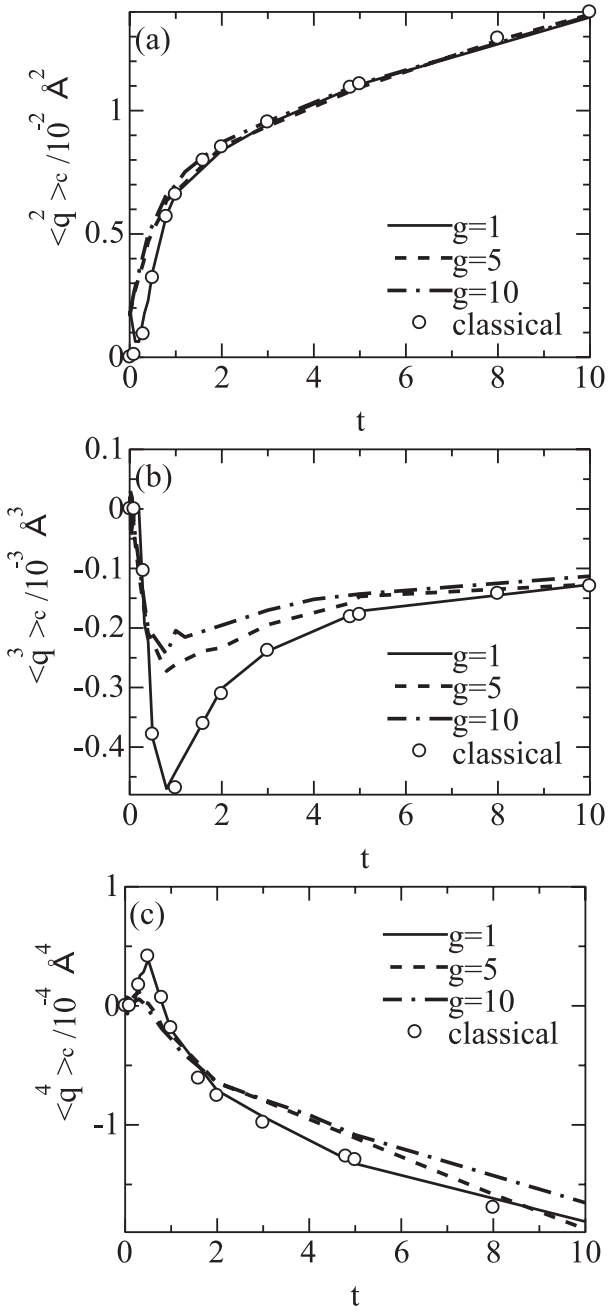

Fig. 7. The temperature dependence of the quantum and classical second (a), third (b), and fourth (c) order cumulants for various g; $g = 1$ (solid lines), $g = 5$ (dashed lines), $g = 10$ (dash-dotted lines) and classical results (circles): t is reduced temperature.

$$G(k) = \langle \exp(2ikq) \rangle = \int_{-\infty}^{\infty} \exp(2ikq) P(q)\, dq. \quad (22)$$

This function can be written in the cumulant expansion as far as that expansion converges. Actually it rapidly converges in weak anharmonic systems;

$$G(k) = \exp\left\{ -2k^2 \langle q^2 \rangle_c + \frac{2}{3} k^4 \langle q^4 \rangle_c - \cdots \right\} \times \exp\left\{ i\left(k\langle q \rangle_c - \frac{4}{3} k^3 \langle q^3 \rangle_c + \cdots \right) \right\}. \quad (23)$$

Equation (22) can be applied to any strongly anharmonic systems, whereas eq. (23) can only be applied to weak anharmonic systems. Now we separately calculate $|G(k)|$ and phase $\phi(k)$

$$|G(k)| = \sqrt{\langle \cos(2kq) \rangle^2 + \langle \sin(2kq) \rangle^2} \approx \exp\left\{ -2k^2 \langle q^2 \rangle_c + \frac{2}{3} k^4 \langle q^4 \rangle_c - \cdots \right\}, \quad (24)$$

$$\phi(k) = \tan^{-1}\left(\frac{\langle \sin(2kq) \rangle}{\langle \cos(2kq) \rangle} \right) \approx k\langle q \rangle_c - \frac{4}{3} k^3 \langle q^3 \rangle_c + \cdots. \quad (25)$$

We also use another form

$$(G_x, G_y) = (\mathrm{Re}\, G, \mathrm{Im}\, G). \quad (26)$$

The damping strength $|G(k)|$ dominates the envelop of EXAFS oscillation function $\chi(k)$, and the phase $\phi(k)$ appears in sinusoidal function of $\chi(k)$. The trajectories of (G_x, G_y) on the complex plane contains useful information on the thermal factor $G(k)$. Figures 8–10 show (a) the amplitudes $|G(k)|$, (b) the phases $\phi(k)$, and (c) (G_x, G_y) on the complex plane at three temperatures $T = 15.2$ K (Fig. 8), 242 K (Fig. 9), 1520 K (Fig. 10). For the symmetric potential $c = 0$, $G(k)$ has to be real and the trajectory of (G_x, G_y) oscillates just on the real axis which is not plotted here. At low temperature $T = 15.2$ K (Fig. 8), as c decreases, the thermal damping $|G(k)|$ get smaller because of the large tunneling probability. The phase $\phi(k)$ for both $c = 1$ and 4 show monotonically increasing function of k. In the complex plane, the trajectory for $c = 4$ is far from real axis in comparison with that for $c = 1$. This means that the trajectory on complex plane can be an indicator of the anharmonicity of the atomic pair potential.

At $T = 242$ K (Fig. 9), the characteristic feature for the thermal factor for the double-well potential appears in the case of $c = 0$, "beat" in $|G(k)|$ at $k = 10$ Å^{-1}. In the case of $c = 1$, $|G(k)|$ behaves like "beat" but not so clearly. On the other hand, $|G(k)|$ for $c = 4$ is different from the others; that is smooth, because it has only single potential well (see Fig. 1). The phase for $c = 1$ increases as k and shows an inflection point around $k = 10$ Å^{-1} where the amplitude $|G(k)|$ has an local minimum. In the large asymmetric case ($c = 4$), the amplitude decreases and the phase increases monotonically. In the complex plane, trajectory for $c = 4$ is far from real axis in comparison with $c = 1$ because of large asymmetry of atomic pair potential. The trajectory is on the real axis for $c = 0$. At high temperature $T = 1520$ K (Fig. 10), the amplitude $|G(k)|$ shows "beat" for $c = 0$, 1, and 4 at 8 Å^{-1} (arrow A in Fig. 10) which is smaller than the "beat" for 242 K (10 Å^{-1} in Fig. 9). In Fig. 10, the $|G(k)|$ shows another "beat" at 17 Å^{-1} (arrow B). The "beat" can be related to the small difference in the distances to the scatterers[23)]

$$2k\Delta r = (2n + 1)\pi, \quad (n = 0, 1, 2, \ldots) \quad (27)$$

where Δr is the small difference in the interatomic distances. In the present asymmetric double-well system $\Delta r = 0.2$ Å, so that the "beat" is expected at $k \cong 8.0$ Å^{-1} which is consistent with our result at 1520 K, where the quantum tunneling effect can be neglected. We also observe the "beat" for $c = 4$ but it is not so pronounced. The phase for

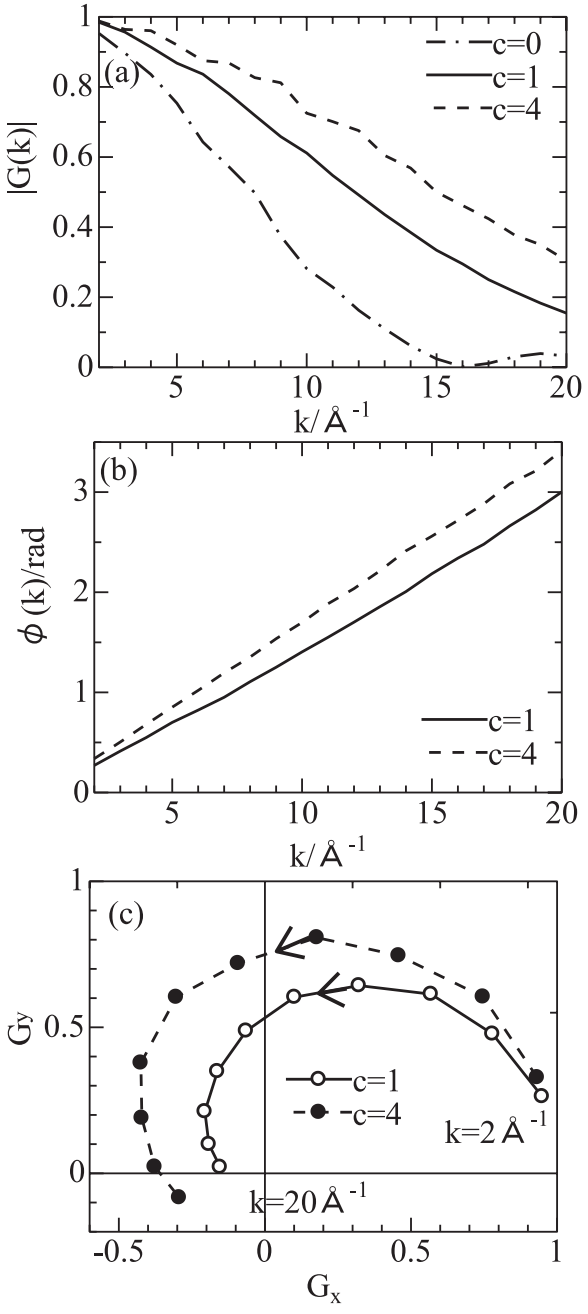

Fig. 8. The amplitudes $|G(k)|$ (a), the phases $\phi(k)$ (b), and complex plane expression (c) in the thermal damping function $G(k)$ of EXAFS at temperature 15.2 K for three different potentials. The black and white dots in (c) are plotted with 2 Å^{-1} intervals.

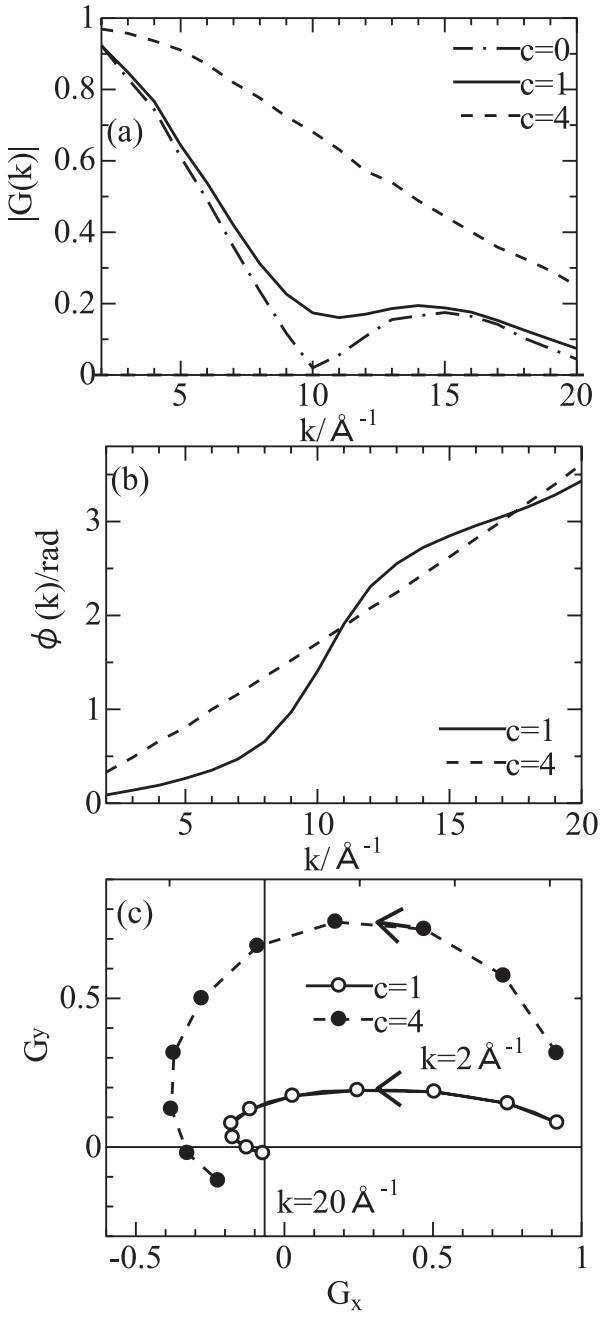

Fig. 9. The amplitudes $|G(k)|$ (a), the phases $\phi(k)$ (b), and complex plane expression (c) in the thermal damping function $G(k)$ of EXAFS at temperature 242 K for three different potentials. The black and white dots in (c) are plotted with 2 Å^{-1} intervals.

$c = 1$ shows steps at 8 Å^{-1}(arrow A) and 17 Å^{-1}(arrow B), where the jump is about π. The "beat" is more remarkable at high temperature where the classical picture works well than at low temperature. In Fig. 10(c), we plot (G_x, G_y) near the real axis for $c = 1$ but we see that $G_y \neq 0$ because $P(q)$ is not a complete symmetric function. The phase of $G(k)$ rapidly changes near at 8 Å^{-1}(arrow A) and 17 Å^{-1}(arrow B) where the "beat" occurs. The characteristic feature in Figs. 10(a) and 10(b) are understood from the trajectory of (G_x, G_y) for the quantum calculation. From 2 to 10 Å^{-1} it is nearly on a straight line crosses the imaginary axis at 8 Å^{-1} almost parallel to the real axis. So that we find $|G(k)|_{\min}$ at $\sim$8 Å^{-1}. From 12 to 20 Å^{-1} the trajectory is again on a straight line quite close to the origin, which gives small $|G(k)|$ as observed in Fig. 10(a) whereas gives large change in $\phi(k)$ [see Fig. 10(b)].

Next, we discuss the validity of the classical approximation and the cumulant expansion of the damping function $G(k)$. Figure 11 shows (a) the amplitude $|G(k)|$, (b) phase $\phi(k)$ and (c) complex plane expression of the thermal damping function for the quantum path-integral (solid line) and the classical (dashed line) calculation at $T = 15.2$ K for $c = 1$. The cumulant expansion up to fourth order (dash-dotted line) is also shown. As the classical approximation is poor at low temperature, the amplitude $|G(k)|$ in the classical approximation really gives a poor agreement with the quantum path-integral calculation because the probability density $P(q)$ is strongly affected by tunneling. On the other

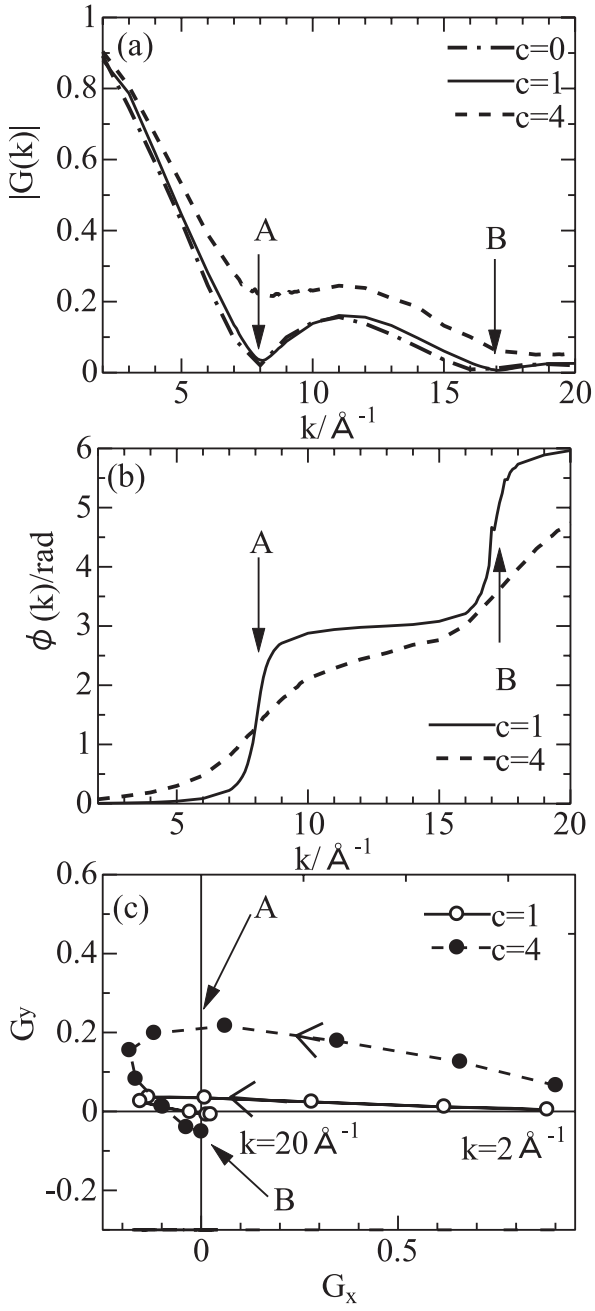

Fig. 10. The amplitudes $|G(k)|$ (a), the phases $\phi(k)$ (b), and complex plane expression (c) in the thermal damping function $G(k)$ of EXAFS at temperature 1520 K for three different potentials. The arrows A and B are the position where the "beat" is observed. The black and white dots in (c) are plotted with 2 Å^{-1} intervals.

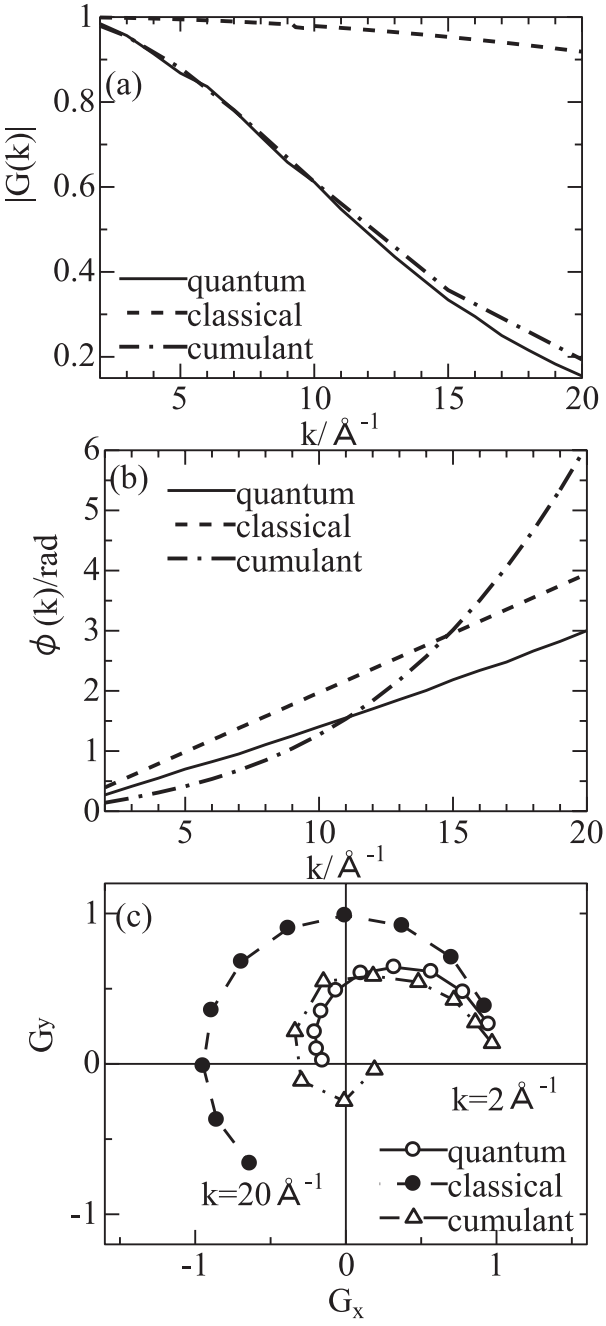

Fig. 11. The amplitude $|G(k)|$ (a) and phase $\phi(k)$ (b) and complex plane expression (c) in thermal damping function $G(k)$ of EXAFS for the quantum (solid line) and the classical (dashed line) approaches at $T = 15.2$ K for $c = 1$. The cumulant expansion up to fourth order (dash-dotted line) is also shown.

hands, the cumulant expansion gives good agreement with the quantum path-integral calculation. The quantum path-integral calculation for the phase $\phi(k)$ monotonically increases, and the classical result is similar to the quantum result, but is a little larger. On the other hand, the cumulant expansion is quite good up to $k = 12$ Å^{-1}, whereas it gets poor above 12 Å^{-1}. In the complex plane expression (c), the trajectory for the classical approximation is similarly expanded from the trajectory for the quantum path-integral approach. This is the reason why they show similar behavior in $\phi(k)$ but different behavior in $|G(k)|$. The trajectory for the cumulant approximation is quite close to the quantum trajectory, which gives rise to the nearly same $|G(k)|$, whereas $G(k)$ moves more rapidly for the cumulant approximation, in particular at large k, than for the quantum method, which results in the large difference of $\phi(k)$. In contrast to the quantum calculation, the classical calculation gives a trajectory is nearly on a circle around the origin: This gives $|G(k)| \sim$ const. in that region.

Figure 12 shows (a) the amplitude $|G(k)|$, (b) phase $\phi(k)$ and (c) complex plane expression for the quantum path-integral (solid line) and the classical (dashed line) calculation at $T = 242$ K for $c = 1$. The cumulant expansion up to fourth order (dash-dotted line) is also shown. In the amplitude $|G(k)|$, these three calculations are in good agreement in the low wavenumber region ($\lesssim 8$ Å^{-1}). In

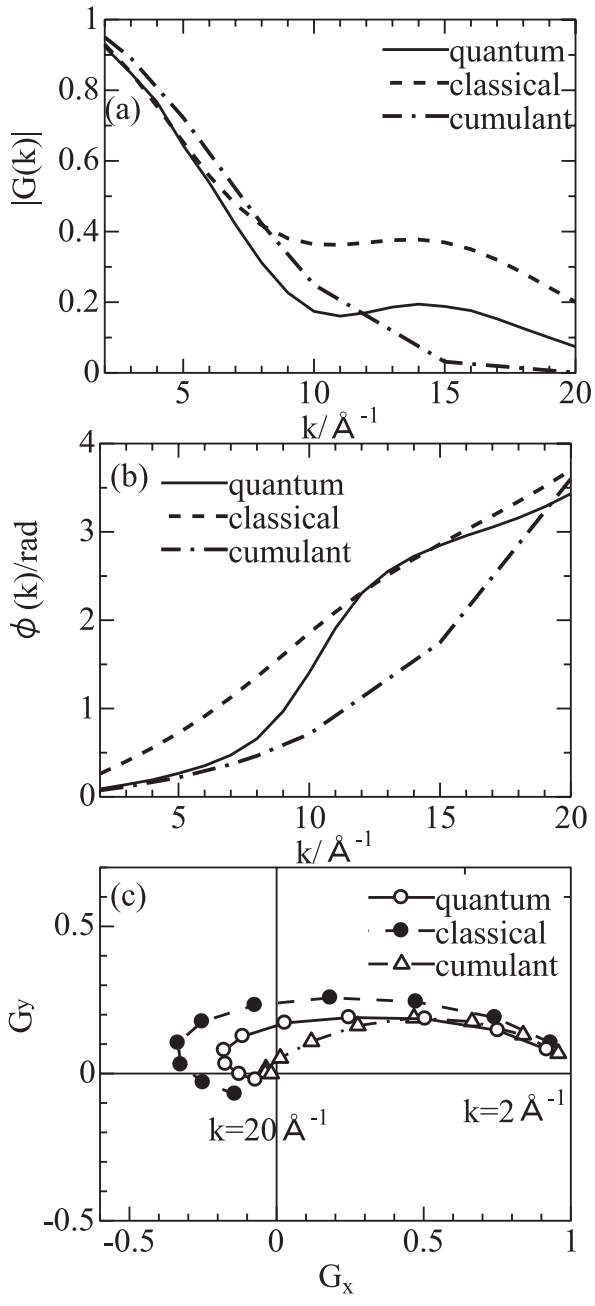

Fig. 12. The amplitude $|G(k)|$ (a), phase $\phi(k)$ (b) and complex plane expression (c) in thermal damping function $G(k)$ of EXAFS for the quantum (solid line) and the classical (dashed line) calculation at $T = 242\,\mathrm{K}$ for $c = 1$. The cumulant expansion up to fourth order (dash-dotted line) is also shown.

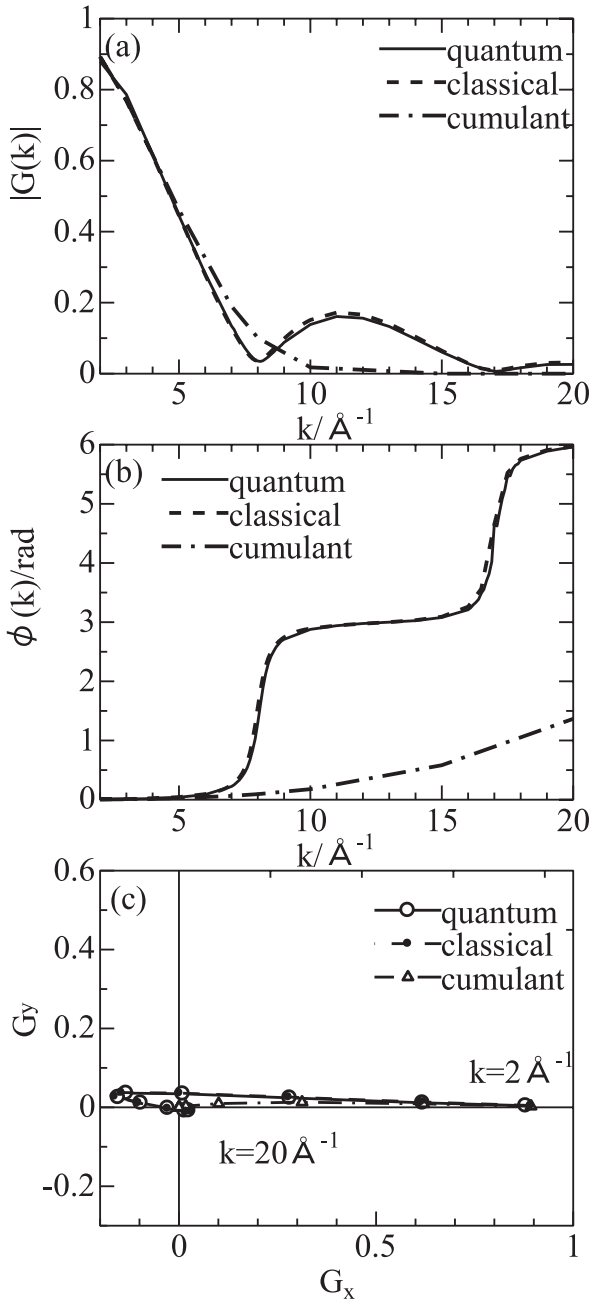

Fig. 13. The amplitude $|G(k)|$ (a), phase $\phi(k)$ (b) and complex plane expression (c) in thermal damping function $G(k)$ of EXAFS for the quantum (solid line) and the classical (dashed line) calculation at $T = 1520\,\mathrm{K}$ for $c = 1$. The cumulant expansion up to fourth order (dash-dotted line) is also shown.

the high wavenumber region ($\gtrsim 15\,\mathrm{Å}^{-1}$), the classical approximation and the cumulant expansion are rather poor but the former can predict the "beat". In the phase $\phi(k)$, neither the cumulant expansion nor the classical approximation are poor as observed for the symmetric double-well potential.[11] In the complex plane expression, the classical approximation deviates from the quantum curve. The cumulant expansion gives good result in low wavenumber region but it cannot predict quantum behavior in high wavenumber region: Higher order cumulants should be taken into account in this region. The observed behavior is well explained by the trajectories in (c), where from 10 to $16\,\mathrm{Å}^{-1}$ both the quantum and the classical trajectories are on different circles around the origin.

Figure 13 shows (a) the amplitude $|G(k)|$, (b) phase $\phi(k)$ and (c) complex plane expression in the thermal damping function of EXAFS for the quantum path-integral (solid line) and the classical (dashed line) calculation at $T = 1520\,\mathrm{K}$ for $c = 1$. The cumulant expansion up to fourth order (dash-dotted line) is also shown. At such high temperature, the bare potential and the local effective potential is almost the same and the classical approximation gives a good result in $|G(k)|$ and $\phi(k)$. The cumulant expansion up to fourth order cannot predict the "beat". The reason why the cumulant calculation fails to predict the "beat" is easily understood from the trajectory shown in (c).

4. Conclusion

The real space method based on finite temperature path integral theory has been applied to the EXAFS thermal factors for strongly anharmonic systems. The path integral calculation shows quite different distribution function $P(q)$ from the classical one, in particular, for $c = 0$, (the symmetric double-well potential). It has a peak at $q = 0$ Å because of tunneling effect through the potential barrier. The asymmetric potentials give rise to peak shift from the potential bottom.

The two characteristic features are observed in the asymmetric double-well potential:

(1) The amplitude of EXAFS damping function $|G(k)|$ shows "beat" both for symmetric and asymmetric potentials. We can estimate the distance between the two bottoms of effective potential from the wavenumber where "beat" occurs at the basis of EXAFS study on high temperature.

(2) In the temperature dependence of third (fourth) order cumulants, there is minimum (maximum) point (T_m) which is characteristic for the double-well potential; T_m reflects the asymmetric parameter c.

These features can be applied to experimental analyses, e.g., $PrOs_4Sb_{12}$. If we observe the "beat" behavior in the envelop function of EXAFS for Pr–Os pairs, that indicates directly Pr–Os is stretching in the double-well potential inside Os_4Sb_{12} cage: We can estimate the separation of the bottom positions from the wavenumber at the "beat". Furthermore, if we observe the minimum point T_m in the temperature dependence of third-order cumulant for Pr–Os pair, the double-well potential is asymmetric: We can estimate the asymmetric parameter c from T_m.

The complex plane expression is introduced to get insight to the specific feature of the "beat". When the distance $|G(k)|$ oscillates, we expect the "beat".

The "beat" analysis has been performed experimentally for Cu and CuO:[24] The "beat" is observed at $k = 9$ Å^{-1} for CuO which can be related to the small difference in the Cu–O interatomic distances. The good agreement was observed between small difference in the interatomic distance obtained. More recently, Mustre de Leon *et al.* showed the beat analyses: They observed the "beat" at $k = 12$ Å^{-1}. They also use the double-well potential for the EXAFS analysis for axial Cu–O pairs in $YBa_2Cu_3O_7$.[10] Their analyses are based on the classical approach even in the low temperature region. The present path integral calculations include the quantum tunneling effects, and they can estimate the temperature range where the classical approximation works safely.

1) G. Beni and P. M. Platzman: Phys. Rev. B **14** (1976) 1514.
2) J. M. Tranquada and R. Ingalls: Phys. Rev. B **28** (1983) 3520.
3) T. Fujikawa and T. Miyanaga: J. Phys. Soc. Jpn. **62** (1993) 4108.
4) T. Miyanaga and T. Fujikawa: J. Phys. Soc. Jpn. **63** (1994) 1036.
5) T. Miyanaga and T. Fujikawa: J. Phys. Soc. Jpn. **63** (1994) 3683.
6) T. Fujikawa, M. Yimagawa and T. Miyanaga: J. Phys. Soc. Jpn. **64** (1995) 2047.
7) P. Rennert: *Proc. 7th Conf. X-Ray Absorption in Fine Structure*, Jpn. J. Appl. Phys. **32** (1993) Suppl. 32-2, p. 19.
8) A. I. Frenkel and J. J. Rehr: Phys. Rev. B **48** (1993) 585.
9) T. Yokoyama, T. Satsukawa and T. Ohta: Jpn. J. Appl. Phys. **28** (1989) 1905.
10) J. Mustre de Leon, S. D. Conradson, I. Bastic, A. R. Bishop, I. D. Raistrick, M. C. Aronson and F. H. Garzon: Phys. Rev. B **45** (1992) 2447.
11) T. Fujikawa, T. Miyanaga and T. Suzuki: J. Phys. Soc. Jpn. **66** (1997) 2897.
12) T. Miyanaga and T. Fujikawa: J. Phys. Soc. Jpn. **67** (1998) 2930.
13) R. P. Feynman: *Statistical Mechanics* (Benjamin, Reading, MA, 1972).
14) A. Cuccoli, R. Giachetti, V. Tognetti, R. Vaia and P. Verrucchi: J. Phys.: Condens. Matter **7** (1995) 7891.
15) R. P. Feynman and H. Kleinert: Phys. Rev. B **33** (1986) 7647.
16) T. Miyanaga, T. Suzuki and T. Fujikawa: J. Synchrotron Radiat. **7** (2000) 95.
17) T. Yokoyama: Phys. Rev. B **57** (1998) 3423.
18) S. a Beccara, G. Dalba, P. Fornasini, R Grisentini, F. Pederiva and A. Sanson: Phys. Rev. B **68** (2003) 140301.
19) T. Miyanaga, D. Diop, S. Ikeda and H. Kon: Ferroelectrics **274** (2002) 41.
20) D. L. Freeman and J. D. Doll: Annu. Rev. Phys. Chem. **47** (1996) 43.
21) T. Goto, Y. Nemoto, K. Sakai, T. Yamaguchi, M. Akatsu, T. Yanagisawa, H. Hazama and K. Onuki: Phys. Rev. B **69** (2004) 180511.
22) E. D. Crozier, N. Alberding, K. R. Bauchspiess, A. J. Seary, and S. Gygax: Phys. Rev. B **36** (1987) 8288.
23) E. D. Crozier: Physica B **158** (1989) 14.
24) G. Martens, P. Rabe, N. Schwentner and A. Werner: Phys. Rev. Lett. **39** (1977) 1411.